BIOCHEMISTRY
including biophysical chemistry & molecular biology

Article

pubs.acs.org/biochemistry

Effects of Point Substitutions on the Structure of Toxic Alzheimer's β-Amyloid Channels: Atomic Force Microscopy and Molecular Dynamics Simulations

Laura Connelly,[†] Hyunbum Jang,[‡] Fernando Teran Arce,[†] Srinivasan Ramachandran,[†] Bruce L. Kagan,[§] Ruth Nussinov,*[,‡,∥] and Ratnesh Lal*[,†]

[†]Departments of Bioengineering and Mechanical and Aerospace Engineering and Material Science Program, University of California, San Diego, La Jolla, California 92093, United States

[‡]Basic Science Program, SAIC-Frederick, Inc., Center for Cancer Research Nanobiology Program, Frederick National Laboratory for Cancer Research, Frederick, Maryland 21702, United States

[§]Department of Psychiatry, David Geffen School of Medicine, Semel Institute for Neuroscience and Human Behavior, University of California, Los Angeles, California 90024, United States

[∥]Department of Human Molecular Genetics and Biochemistry, Sackler School of Medicine, Tel Aviv University, Tel Aviv 69978, Israel

Supporting Information

ABSTRACT: Alzheimer's disease (AD) is a misfolded protein disease characterized by the accumulation of β-amyloid (Aβ) peptide as senile plaques, progressive neurodegeneration, and memory loss. Recent evidence suggests that AD pathology is linked to the destabilization of cellular ionic homeostasis mediated by toxic pores made of Aβ peptides. Understanding the exact nature by which these pores conduct electrical and molecular signals could aid in identifying potential therapeutic targets for the prevention and treatment of AD. Here using atomic force microscopy (AFM) and molecular dynamics (MD) simulations, we compared the imaged pore structures with models to predict channel conformations as a function of amino acid sequence. Site-specific amino acid (AA) substitutions in the wild-type $A\beta_{1-42}$ peptide yield information regarding the location and significance of individual AA residues to its characteristic structure−activity relationship. We selected two AAs that our MD simulation predicted to inhibit or permit pore conductance. The substitution of Phe19 with Pro has previously been shown to eliminate conductance in the planar lipid bilayer system. Our MD simulations predict a channel-like shape with a collapsed pore, which is supported by the AFM channel images. We suggest that proline, a known β-sheet breaker, creates a kink in the center of the pore and prevents conductance via blockage. This residue may be a viable target for drug development studies aiming to inhibit Aβ from inducing ionic destabilization toxicity. The substitution of Phe20 with Cys exhibits pore structures indistinguishable from the wild type in AFM images. MD simulations predict site 20 to face the solvated pore. Overall, the mutations support the previously predicted β-sheet-based channel structure.

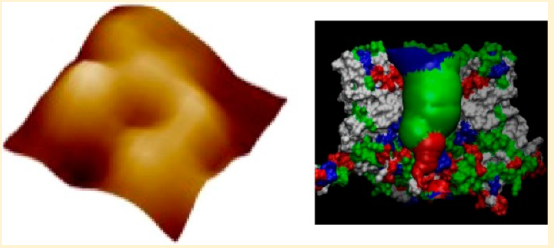

The β-amyloid (Aβ) peptide is the primary component of extracellular fibrillar deposits, termed amyloid plaques, found post-mortem in brain tissues of patients with Alzheimer's disease (AD).[1,2] These peptides are able to form distinct polymorphic structures, ranging from globular oligomers to mature fibrils.[2−4] Fibrillar structures have been widely investigated through in vivo and in vitro studies,[5−7] but interest has gradually shifted toward smaller oligomers, as a growing body of evidence points to the structures formed by these oligomers as the pathogenic agents involved at the onset of AD.[4,8−10] More recently, the amyloid channel hypothesis that postulates the presence of pore structures, formed by small oligomers that are able to disrupt cellular ionic homeostasis, is emerging as one of the principal hypotheses associated with pathogenesis.[9,11−14]

Point mutations in the amyloid precursor protein (APP) located within or in the vicinity of the full-length Aβ peptide have been linked to disease.[15,16] Of particular interest is the mutations clustered around a central hydrophobic cluster of Aβ. These include the E22Q point mutation, associated with hereditary cerebral hemorrhage by amyloidosis of the Dutch type (HCHWA-D); the E22G mutation, known as the arctic mutation; and the A21G mutation, known as the Flemish mutation, related to cerebral amyloid angiopathy (CAA) and presenile dementia.[15,16] Proline mutations in this central region have attracted particular interest, as they have been shown to

Received: February 25, 2012
Revised: March 12, 2012
Published: March 13, 2012

dx.doi.org/10.1021/bi300257e | *Biochemistry* 2012, 51, 3031−3038

suppress β-sheet and fibril formation in the Aβ peptide and fragments thereof.[17−20] The β-sheet conformation in individual Aβ peptides has been modeled as being essential to the formation of cell membrane-penetrating pores.[21−23] Cysteine mutations have also been investigated in this central region, with L17C and V18C point mutations resulting in a decreased level of fibril formation; F20C produced a degree of fibril formation similar to that of wild-type $A\beta_{1-40}$.[24]

Using molecular dynamics (MD) simulations of pores formed by $A\beta_{17-42}$ (p3) peptides inside lipid bilayers, we have previously suggested that the central cluster of the full-length $A\beta_{1-42}$ sequence is located in the β-sheet lining the pore region.[23,25−27] According to these MD simulations using the U-shaped peptides with the β-strand−turn−β-strand motif, the more hydrophilic N-terminus lines the pore while the more hydrophobic C-terminus lines the lipid bilayer. In recent studies, an F19P point substitution in the p3 peptide (p3-F19P) and full-length $A\beta_{1-42}$ was suggested to form collapsed pores, which were unable to conduct ionic currents across lipid bilayers.[25,28] In this paper, we have used atomic force microscopy (AFM) and MD simulations to investigate the effect of F19P and F20C mutations on the pore structures formed by the full-length $A\beta_{1-42}$ peptide inside lipid bilayers. We correlate these point substitutions in the amino acid sequence of Aβ with changes in the pore structure, the propensity for β-sheet formation, variations in the peptide−peptide and peptide−lipid interaction energies, and the different energy landscape for ions inside the pores. Adding to previous data, this new study helps elucidate the structure−activity relationship of Aβ as a toxic pore and provides additional evidence that Aβ pores destabilize cellular ionic homeostasis.

MATERIALS AND METHODS

Materials. For storage, peptides were solubilized in a 1% NH_4OH ultrapure solution at a concentration of 1 mg/mL, separated into aliquots, and stored at −80 °C. Aliquots were thawed once and used immediately. Molecular biology grade water from Fisher Scientific (Pittsburgh, PA) was used for sample preparations. Electrolyte solutions at pH 7.4, containing 150 mM KCl and 1 mM $MgCl_2$ and buffered with 10 mM HEPES, were used for AFM imaging in liquid. The phospholipid 1,2-dioleoyl-*sn*-glycero-3-phosphocholine (DOPC) was purchased from Avanti Polar Lipids (Alabaster, AL). Peptides were purchased from Bachem (Torrance, CA).

Atomic Force Microscopy (AFM) Imaging. Multimode AFM systems equipped with a Nanoscope IIIa controller and a Nanoscope IV controller (Bruker, Santa Barbara, CA) were used. Oxide-sharpened cantilevers (Asylum Research, Santa Barbara, CA) with nominal spring constants (k_n) of 0.02 or 0.08 N/m were employed. For experiments performed in liquid, a fluid cell (Bruker) was utilized. Before each experiment, the fluid cell was washed with detergent (∼5 min) and vigorously rinsed with a constant stream of deionized water. The fluid cell was then sonicated for 2 min in molecular grade water, dried with a Kim wipe, and used immediately. In some cases, the liquid cell, with a cantilever mounted, was cleaned with UV and ozone for 30 min. Images in liquid were acquired in tapping mode at scan frequencies of 0.5−3.0 Hz and drive amplitudes of <100 mV. The cantilever oscillation frequency was 5−10 kHz. Imaging of dried fiber samples was performed in air in contact mode. Some of the AFM images were low-pass filtered to remove noise. Image analysis was performed using the Bruker Nanoscope software. The average outer diameters of all pores were determined using the "Analyze Width" and "Circular Dimensions" options included in NanoScope version 31. The "Analyze Width" feature collects heights of a selected area, applies a Gaussian low-pass filter to remove noise, and produces a histogram of heights, which can be visually correlated with features of the selected area according to their height. On the basis of this information, we selected a region enclosing a pore and used the "Circular Dimensions" option to find the average outer diameter of the pore, which was selected manually from the histogram of heights and associated image. Tip deconvolution and tip shape factors were not taken into account in this analysis; therefore, the outer diameter values provided in the analysis are overestimated.

Sample Preparation. DOPC bilayers were formed by drying 60 μL of DOPC (5 mg/mL) dissolved in chloroform in a rotovap and replacing the vacuum with Ar. The dried lipid cake was hydrated with 300 μL (1 mg/mL) of an electrolyte solution containing 150 mM KCl and 1 mM $MgCl_2$ buffered with 10 mM HEPES (pH 7.4) and vortexed gently. The liposomes formed via this procedure were sonicated for 5 min in an ice bath. Following thawing of the F19P and F20C mutant solutions, aliquots were sonicated for ∼1 min and immediately incorporated into liposomes of DOPC. To incorporate the peptides into the lipid bilayer, we combined DOPC liposomes and peptide at a 20:1 weight ratio and sonicated in an ice bath for 10 min. The liposome/peptide mixture was allowed to adhere to freshly cleaved mica for 30 s and washed 10 times with the electrolyte solution. Bilayers were imaged at room temperature. For imaging of fibers, aliquots of the peptide in water were thawed and incubated without being shaken for 72 h at 37 °C. The aliquots were then diluted and deposited on fresh mica and allowed to dry overnight.

Molecular Dynamics Simulations. To model Alzheimer's Aβ channels, we conceptually designed an Aβ barrel in an annular shape using two U-shaped monomers: one is $A\beta_{1-42}$ as defined in the fibril on the basis of hydrogen−deuterium exchange nuclear magnetic resonance (NMR) data, side chain packing constraints from pairwise mutagenesis, solid-state NMR, and EM [Protein Data Bank (PDB) entry 2BEG];[29] the other is $A\beta_{1-40}$ based on the solid-state NMR model of small protofibrils.[30] However, both conformers miss the N-terminal coordinates because of conformational disorder. We used the N-terminal coordinates obtained from the solution NMR structure of $A\beta_{1-16}$, however, with the Zn^{2+} removed (PDB entry 1ZE7).[31] This structure was used to fill in the missing N-terminal portion of the peptides. For each combination of the N-terminal structure with the U-shaped motifs, two $A\beta_{1-42}$ conformers were generated. Conformer 1 has a turn at Ser26−Ile31, and conformer 2 has a turn at Asp23−Gly29.[32,33] In the latter conformer, two C-terminal residues, Ile41 and Ala42, were added to create $A\beta_{1-42}$. For the sake of convenience, we divided both Aβ conformers into four domains: N-terminal chain (residues 1−16 and 1−8 for conformers 1 and 2, respectively), pore-lining β-strand (residues 17−25 and 9−22 for conformers 1 and 2, respectively), turn (residues 26−31 and 23−29 for conformers 1 and 2, respectively), and C-terminal β-strand (residues 32−42 and 30−42 for conformers 1 and 2, respectively).

For both conformers, we replaced two phenylalanine residues, Phe19 and Phe20, with Pro19 and Cys20, respectively, creating coordinates for F19P and F20C point mutants (Figure 1A,B). Now we have six $A\beta_{1-42}$ monomer conformations, the wild type and two mutants from each conformer, which are subjected to the Aβ barrel simulations. These Aβ conformers

dx.doi.org/10.1021/bi300257e | Biochemistry 2012, 51, 3031−3038

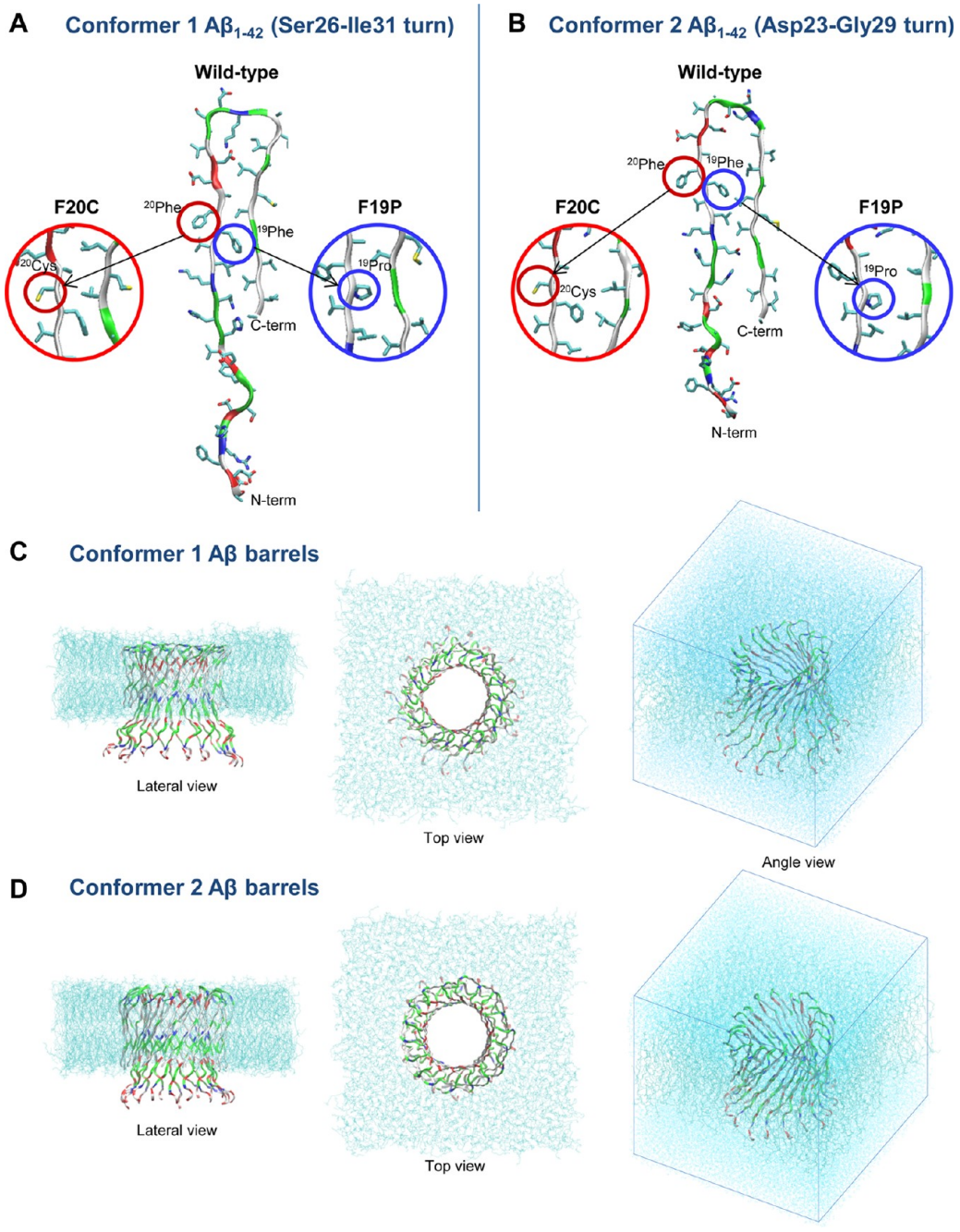

Figure 1. Monomer conformations of the Aβ_{1-42} wild type and F19P and F20C mutants with different turns at (A) Ser26−Ile31 (conformer 1) and (B) Asp23−Gly29 (conformer 2). Starting points of the Aβ_{1-42} barrels embedded in the lipid bilyer for the MD simulations for (C) conformer 1 and (D) conformer 2 Aβ_{1-42} barrels. Waters were removed for the sake of clarity in the lateral and top views, but they are depicted as cyan dots in the simulation box in the angle view. In the peptide ribbon, hydrophobic residues are colored white, polar and Gly residues are green, positively charged residues blue, and negatively charged residues red.

were inclined ~37° relative to the pore axis[26] and then rotated 18 times with respect to the pore axis creating Aβ barrels (Figure 1C,D). These Aβ barrels were embedded in an anionic lipid bilayer containing 1,2-dioleoyl-*sn*-glycero-3-phosphoserine (DOPS) and 1-palmitoyl-2-oleoyl-*sn*-glycero-3-phosphoethanolamine (POPE) (mole ratio of 1:2). The anionic lipid bilayer containing a total of 420 lipids constitutes the unit cell with TIP3P waters, added at both sides. The system contains Mg^{2+}, K^{+}, Ca^{2+}, and Zn^{2+} at the same concentration (25 mM) to satisfy a total cation concentration of ~100 mM. CHARMM[34] was used to construct the set of starting points and to relax the systems to a production-ready stage. For production runs, the NAMD code[35] on the Biowulf cluster (http://biowulf.nih.gov) at the National Institutes of Health was used for the starting point with the same CHARMM27 force field. Averages were taken after 20 ns, discarding initial transients. Analysis was performed with the CHARMM programming package.[34] More detailed simulation methods can be found elsewhere.[25−27,32,33,36,37]

RESULTS

Atomic Force Microscopy Analysis of F19P and F20C Pore Morphologies. High-resolution AFM images of F19P

dx.doi.org/10.1021/bi300257e | *Biochemistry* 2012, 51, 3031−3038

and F20C mutants of Aβ_{1-42} incorporated into a DOPC bilayer supported on mica were acquired. When the presence of a single bilayer was confirmed by imaging hole defects with characteristic depths of ~4 nm, high-resolution imaging of the pores was attempted in the vicinity of the defect. The pores produced by the F19P mutant in DOPC bilayers show behavior similar to that of the previously reported full-length wild-type Aβ_{1-42} (Figure 2A).[9,12] The pores could be identified as central dips inside doughnutlike structures, and in some cases, individual subunits appeared as protrusions in the amplitude images (Figure 2B). The pores were seen in the AFM images prior to the removal of noise (Figure S1 of the Supporting Information). The pore structures of F19P are multimeric. Trimers, tetramers, pentamers, and hexamers were observed (Figure 2B and Table S1 of the Supporting Information). Many of the structures observed could not be resolved into individual subunits. These unresolved structures may indicate the presence of globular oligomers or the inability of the AFM tip to resolve the subunits. For the F20C peptide, the protruding structures appeared to be clustered and could be seen within scan areas of 500 nm × 500 nm (Figure 2C and Figure S1 of the Supporting Information). While the majority of the F20C pores were seen as pentamers, wild-type Aβ_{1-42} typically showed a preference for trimeric to hexameric pore conformations (Figure 2D).[9,12] The F20C pore structures were seen in unprocessed AFM images (Figure S1 of the Supporting Information). The distribution of the number of subunits for F19P (n = 16) and F20C (n = 16) did not show a very large variation from the distribution of the wild type (n = 16) (Table S1 of the Supporting Information). For a more statistically significant conclusion of subunit number bias, a larger sample set would be required but was not completed on the basis of these preliminary results.

Height images without noise removal for both F19P and F20C (Figure S1A,C of the Supporting Information), acquired simultaneously with the amplitude images, clearly indicate a pore structure. From AFM images, the average pore diameter (±standard deviation) was 11.3 ± 1.6 nm (n = 16) for wild-type Aβ_{1-42}, 11.2 ± 1.6 nm (n = 16) for F19P, and 7.9 ± 1.4 nm (n = 16) for F20C, as shown in Figure 2E.

The F19P peptide was incubated for 72 h in water at 37 °C, dried on fresh mica, and imaged in air. Fiber formation appeared similar to previously reported images of the wild-type peptide (Figure 3). This incubation and imaging were preformed several times with different batches of the peptide. Each sample set showed fiber formation had occurred.

Molecular Dynamics Modeling of the Pore Morphologies of F19P and F20C. We performed 100 ns explicit all-atoms molecular dynamics (MD) simulations on Aβ barrels, assembled by wild-type Aβ_{1-42} and its F19P and F20C mutants, embedded in an anionic lipid bilayer composed of DOPS and POPE (mole ratio of 1:2). In the lipid bilayer, the Aβ barrels gradually removed the initial frustration in the annular conformation via relaxation of the lipid bilayer. We calculated the interaction energy for each peptide's U-shaped portion with the lipids and then averaged the interaction energy over the number of peptides as a function of the simulation time (Figure S2 of the Supporting Information). The effect of the point mutation is not immediately reflected in the peptide–lipid interaction, because both point mutations occurred in the pore-lining β-strands that face the solvated pore. The lipids are in the proximity of the hydrophobic C-terminal β-strands. However, the point mutations elicit peptide fluctuations during the simulations. In particular, the pore-lining β-strands are less stable

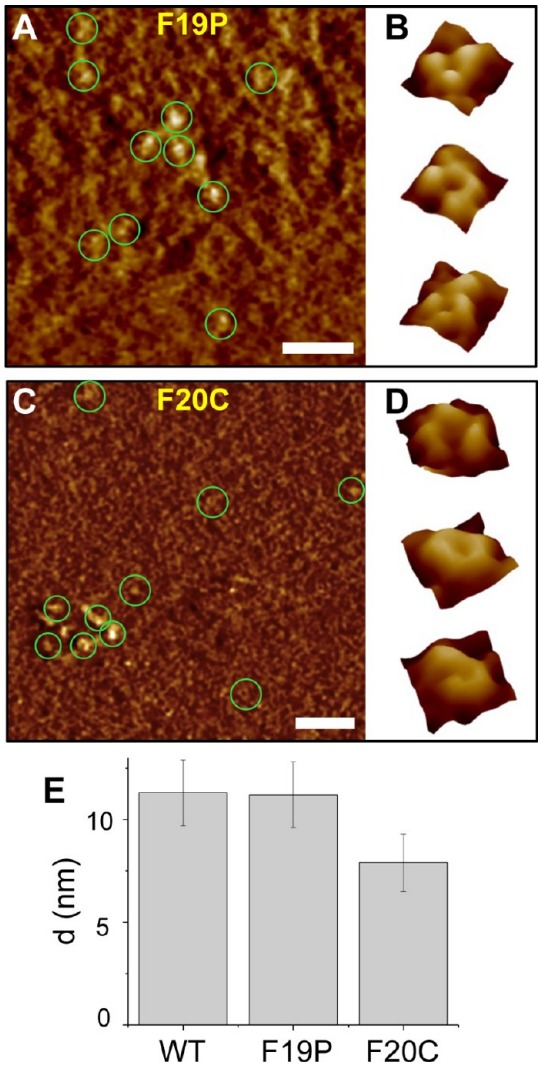

Figure 2. Amplitude AFM images of (A) F19P and (C) F20C mutants of Aβ_{1-42} incorporated into DOPC bilayers on mica. Pores with a central dip were resolved in both processed and unprocessed amplitude, and height images. These amplitude features correlate with height increases in the height image (Figure S1 of the Supporting Information). (B and D) Individual pores from the amplitude images were selected and resolved into multimeric structures: trimers, tetramers, and pentamers. The pores appear characteristic of wild-type Aβ_{1-42} and, as a surface structure image, do not exhibit any indication of a compromised pore structure. A Gaussian low pass of 4 nm once in the x-direction and once in the y-direction was applied to panels A–D to remove noise. Lateral scale bars are 50 nm for panels A and C. Image areas in panel B are 17.46 × 17.46 nm^2, 13.15 × 13.15 nm^2, and 14.54 × 14.54 nm^2 from top to bottom, respectively. Image areas in panel D are 14.00 × 14.00 nm^2, 11.02 × 11.02 nm^2, and 12.50 × 12.50 nm^2 from top to bottom, respectively. (E) Histograms for the average outer pore diameters, d, for wild-type Aβ_{1-42} (n = 16) and its F19P (n = 16) and F20C (n = 16) mutants.

because of the mutated residues than the wild type, increasing the frequency of the overall peptide fluctuations (Figure 4). Large fluctuations in the N-terminal domains indicate that they are disordered chains in the bulk water area, while small fluctuations in the U-shaped portion, including the pore-lining β-strand, the turn, and the C-terminal β-strand, suggest that the U-shaped portions sustain the assembled Aβ barrel structures.

The 18-mer Aβ_{1-42} barrels gradually relax during the simulations. Heterogeneous Aβ barrel structures are presented as cartoons for both conformers for the wild-type and two

dx.doi.org/10.1021/bi300257e | Biochemistry 2012, 51, 3031–3038

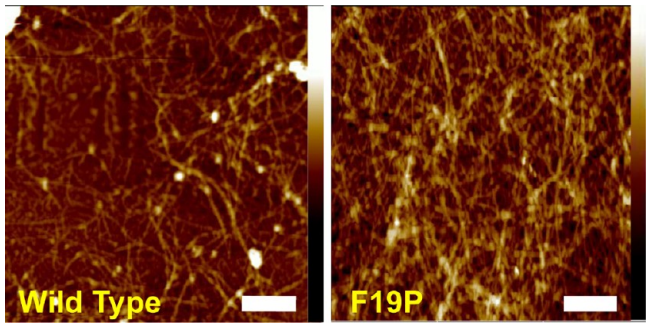

Figure 3. AFM height images of (left) wild-type Aβ_{1-42} and (right) the F19P mutant. Both peptides were incubated in H_2O for 72 h at 37 °C, dried on a fresh mica surface, and imaged in air. Similar fiber formation is seen for both peptides as a variety of sizes are clearly observed. Scale bars are 500 nm, and color scale bars are 50 nm.

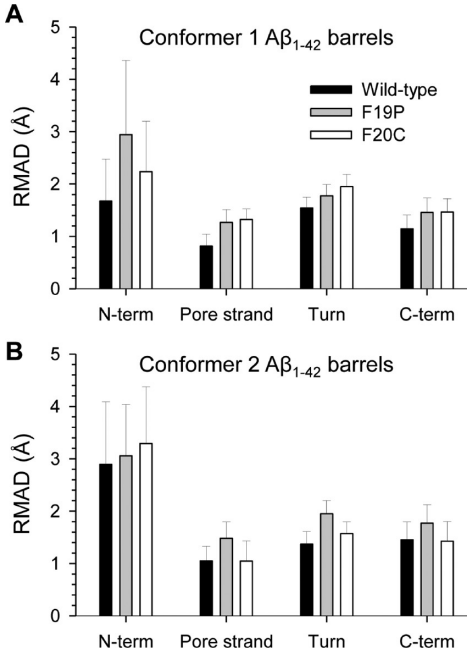

Figure 4. Averaged root-mean-squared deviation, rmsd, from the starting point for C_α atoms of the peptides for the (A) conformer 1 and (B) conformer 2 Aβ_{1-42} barrels. The rmsd was calculated separately for the peptides in the barrels by dividing them into four domains: N-terminal chain, pore-lining β-strand, turn, and C-terminal β-strand.

mutant barrels (Figure 5). The cartoons represent the averaged barrel structures embedding the averaged pore structures as calculated with HOLE.[38] Regardless of the point mutations, the outlines of the Aβ barrels in each conformer are very similar to each other. However, the inner water pore structures are significantly evolved toward a collapsed pore in the mutant barrels. While both conformer 1 and 2 wild-type barrels preserve a fat-tube-like pore, wide enough for active ion conductance, the F19P pores are completely clogged up and collapsed with conformers 1 and 2, respectively. In previous simulations, we observed that the p3-F19P mutant also forms a collapsed pore.[25] Conformer 1 F19P has the same U shape as the p3-F19P mutant but contains an extra N-terminal chain composed of residues 1−16. With F20C mutations, conformer 1 preserves a wide pore while conformer 2 yields a partially collapsed pore. The calculated outer dimensions and pore sizes are summarized (Table 1). Both mutants decrease the outer and pore diameters.

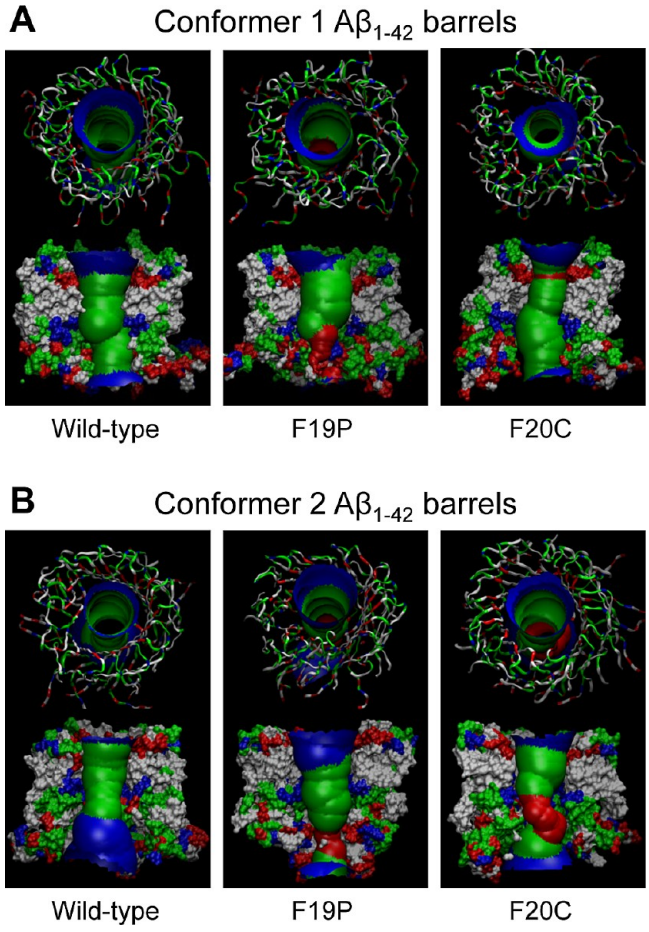

Figure 5. Averaged pore structures calculated with HOLE[38] embedded in the average barrel conformations during the simulations for the (A) conformer 1 and (B) conformer 2 Aβ_{1-42} barrels. In the angle views of the pore structure (top cartoons in each panel), whole barrel structures are shown with the ribbon representation. In the lateral views of the pore structure (bottom cartoons in each panel), cross-sectioned barrels are given in the surface representation. In the peptide, hydrophobic residues are colored white, polar and Gly residues green, positively charged residues blue, and negatively charged residues red. For the pore structures in the surface representation, red denotes pore diameter of d < 1.4 nm, green denotes pore diameter in the range, 1.4 nm ≤ d ≤= 2.0 nm, and blue denotes pore diameter of d > 2.0 nm.

In the F19P barrel, kinks at Pro19 destabilize an inner β-sheet formed by the pore-lining β-strands. As a result, the N-terminal chains containing highly charged residues bind to each other at the channel mouth in the lower bilayer leaflet. These N-terminal chain interactions are responsible for the collapsed pore observed in the F19P mutant barrels. In the wild-type barrels, the N-terminal chain interactions are in the proximity, i.e., mostly interacting with neighboring chains. For example, a contour map representing N-terminal−N-terminal interaction energy for the conformer 1 wild-type barrel shows strong interactions along the diagonal, indicating neighboring chain interactions (Figure 6A). In contrast, for the conformer 1 F19P mutant barrel, contour lines enclosing the strong N-terminal chain interactions are dispersed from the diagonal line, indicating that some chains are cross-linked to other chains at opposite side (Figure 6B). In the F20C barrels, although the mutation did not provide a kink, the conformer 2 barrel produces a smaller pore than the wild type.

dx.doi.org/10.1021/bi300257e | *Biochemistry* 2012, 51, 3031−3038

Table 1. Calculated Outer and Pore Dimensions with a Description of the Pore Status for the Conformer 1 and Conformer 2 $A\beta_{1-42}$ Barrels Composed of the Wild-Type Peptide and Its F19P and F20C Mutants

	conformer 1 $A\beta_{1-42}$ barrel			conformer 2 $A\beta_{1-42}$ barrel		
	wild type	F19P	F20C	wild type	F19P	F20C
outer diameter (nm)	~8.2	~7.7	~7.9	~8.1	~7.6	~8.1
pore height (nm)	~4.1	~5.6	~5.2	~4.5	~5.9	~5.3
pore diameter[a] (nm)	~1.8	~1.5	~1.7	~1.9	~1.7	~1.7
pore status	opened	clogged up	opened	opened	collapsed	partially collapsed

[a]Pore diameters are averaged along the pore axis within the cutoffs defined by the height of the pore.

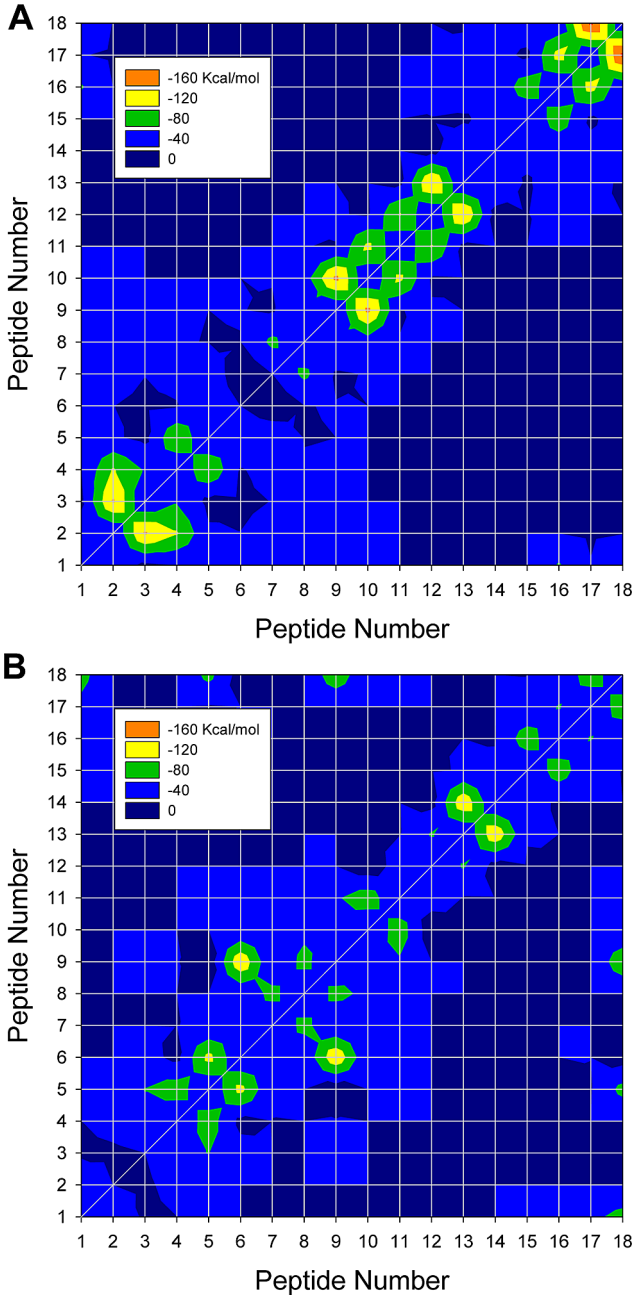

Figure 6. Contour map representing N-terminal–N-terminal chain interaction energies for the conformer 1 (A) $A\beta_{1-42}$ wild-type barrel and (B) F19P mutant barrel.

DISCUSSION

Oligomeric Aβ's role in the pathology of Alzheimer's disease is a growing area of interest. The ability to form fibers and bind Congo red is characteristic of many amyloids, including wild-type Aβ.[39−41] Previous studies of the F19P mutation have reported an inability to form such characteristic fibers and bind Congo red.[17,19] Such differences in the mutant behavior with respect to that of the wild type suggest that the F19P point substitution causes a significant functional change to the peptide. Similarly, we have observed that the F19P mutant of the p3 ($A\beta_{17-42}$) peptide has the ability to elicit changes in the functional behavior of wild-type $A\beta_{17-42}$. The p3-F19P mutant forms collapsed pores that do not allow ion conductance through planar lipid bilayers and do not alter the intracellular Ca^{2+} levels in mouse fibroblast cells.[25] Consistent with that behavior, we have found that the characteristic ion conductance of wild-type $A\beta_{1-42}$ appears to be completely inhibited by the F19P mutant.[28] Although fiber formation, Congo red binding, and conductance of the F19P mutation have been previously reported to prevent amyloidogenic behavior, the effect of the F19P mutation on pore formation has not been examined for full-length Aβ. Following the behavior presented by the p3 peptide, we hypothesized that the pore structure would also be significantly different from that of the wild type for full-length $A\beta_{1-42}$. We sought to determine if F19P prevents insertion into the lipid bilayer or F19P inserts effectively but results in a structurally compromised pore.

Through AFM analysis, we show that F19P is capable of insertion into the bilayer and the pore formation on the bilayer surface is structurally indistinguishable from that of the wild type. AFM image analysis reports that the channels are multimeric as observed in the wild type and have outer diameters similar to that of the wild type. MD simulations show that the overall outer morphologies of the F19P barrels are very similar to that of the wild type. Also, the outer dimensions of the F19P barrels are in the experimental range, although slightly smaller than that of the wild type. In the MD simulations, the outer size measured for the barrels mainly depends on the number of Aβ peptides composing the barrels. Here, we reported the values for 18-mer Aβ barrels. The AFM experiments provide images of channels covering all ranges of channel sizes, but simulated Aβ barrels are limited to sizes of the MD study defined peptide count. MD simulations support the hypothesis that the different functional behavior of wild-type $A\beta_{1-42}$ and F19P channels is due to a modified channel structure. Although the F19P pores are collapsed or clogged, the AFM images do not reveal any change in their internal dimensions because the AFM tip is unable to penetrate deep enough inside the pore to detect a change in the inner pore diameter (Figure 5). Overall through MD simulations and AFM imaging, we found F20C to be indistinguishable from wild-type $A\beta_{1-42}$. This is in good agreement with previous activity reports that both the wild type, p3-F20C, and full-length F20C mutant presented ion conductance by electrophysiology and p3-F20C altered intracellular Ca^{2+} levels.[25,28]

dx.doi.org/10.1021/bi300257e | *Biochemistry* 2012, 51, 3031−3038

The similar structural behavior of pores formed from the wild type as well as F19P and F20C mutants for full-length Aβ_{1-42} and the Aβ_{17-42} fragment in simplified lipid compositions might suggest that the amyloidogenic and nonamyloidogenic pathways can be similarly disruptive to cell membranes. The fact that both pathways are not equally pathogenic to cells is probably due to the presence of additional biochemical processes related to the cellular network and more complex lipid compositions in cellular environments.

Our previous MD simulations suggested that the β-sheet structure is essential to the formation of Aβ pores.[23,25−27,36,37] Our current results further support the idea that pore formation and β-sheet formation are linked. Following previous studies, we suggest two possibilities. (i) The F19P mutation does not completely inhibit β-sheet formation, and therefore, fiber formation may be possible under specific environmental conditions. (ii) Aβ pore formation is not solely reliant on β-sheet formation and involves other mechanisms. Our preliminary AFM results show that F19P, when incubated at 37 °C in water for 72 h, forms fibers (Figure 3). Previous studies that did not observe fiber formation for F19P were conducted under different experimental conditions.[17,20] Furthermore, other studies suggested that a proline mutation[42] or an isostructural mutation[43] at the F19 position may kinetically delay but not prevent oligomer formation. This inconsistency promotes further study of the role of β-sheets in pore formation, such as through additional point mutations and oligomer studies, including incubation times, pH conditions, and temperatures.

CONCLUSIONS

We report a structural study of two point mutations of Alzheimer's disease Aβ_{1-42}. The propensity of the F19P mutation to form channels was found to be similar to that of the wild type through AFM imaging in a DOPC bilayer. MD simulations also predicted channel formation, however, with a collapsed or clogged pore for the two available solid-state NMR-based Aβ_{1-42} conformers. This is in agreement with previous electrophysiology studies, which report no ionic conductance by the F19P mutant. The proline substitution is a β-sheet breaker. This indicates a role for the β-sheet in the Aβ pore and argues for further studies of its contribution and conformation during channel formation. The degree to which the β-sheet was disrupted by this mutation is still unclear and is likely to vary in the heterogeneous channel landscape. Because of the compromised structure and activity of the F19 position and the β-sheet structure, it may be a viable target for AD therapeutic development against pore conductance. Structurally, the F20C mutant was found to behave like the wild type both in MD simulations and in AFM imaging of pore formation.

ASSOCIATED CONTENT

Supporting Information

AFM unprocessed height and amplitude images for F19P and F20C (Figure S1), the distribution of multimeric pores measured for the wild-type Aβ_{1-42} channel and its F19P and F20C mutants (Table S1), and time series of averaged interaction energies of the U-shaped portion of the peptide with lipids (Figure S2). This material is available free of charge via the Internet at http://pubs.acs.org.

AUTHOR INFORMATION

Corresponding Author

*R.N.: e-mail, ruthnu@helix.nih.gov; telephone, (301) 846-5579; fax, (301) 846-5598. R.L.: e-mail, rlal@ucsd.edu; telephone, (858) 822-0384.

Author Contributions

L.C. and H.J. contributed equally to this work.

Funding

This research was supported by the National Institutes of Health (National Institute on Aging Grant AG028709 to R.L.). This project has been funded in whole or in part with Federal funds from the Frederick National Laboratory for Cancer Research, National Institutes of Health, under Contract HHSN261200800001E. This research was supported (in part) by the Intramural Research Program of the National Institutes of Health, Frederick National Lab, Center for Cancer Research.

Notes

The authors declare no competing financial interest.

ACKNOWLEDGMENTS

All simulations were performed using the high-performance computational facilities of the Biowulf PC/Linux cluster at the National Institutes of Health, Bethesda, MD (http://biowulf.nih.gov).

REFERENCES

(1) Blennow, K., de Leon, M. J., and Zetterberg, H. (2006) Alzheimer's disease. *Lancet 368*, 387−403.

(2) Chiti, F., and Dobson, C. M. (2006) Protein misfolding, functional amyloid, and human disease. *Annu. Rev. Biochem. 75*, 333−366.

(3) Arce, F. T., Jang, H., Ramachandran, S., Landon, P. B., Nussinov, R., and Lal, R. (2011) Polymorphism of amyloid β peptide in different environments: Implications for membrane insertion and pore formation. *Soft Matter 7*, 5267−5273.

(4) Butterfield, S. M., and Lashuel, H. A. (2010) Amyloidogenic protein-membrane interactions: Mechanistic insight from model systems. *Angew. Chem. 49*, 5628−5654.

(5) Harper, J. D., Lieber, C. M., and Lansbury, P. T. Jr. (1997) Atomic force microscopic imaging of seeded fibril formation and fibril branching by the Alzheimer's disease amyloid-β protein. *Chem. Biol. 4*, 951−959.

(6) Ionescu-Zanetti, C., Khurana, R., Gillespie, J. R., Petrick, J. S., Trabachino, L. C., Minert, L. J., Carter, S. A., and Fink, A. L. (1999) Monitoring the assembly of Ig light-chain amyloid fibrils by atomic force microscopy. *Proc. Natl. Acad. Sci. U.S.A. 96*, 13175−13179.

(7) Sipe, J. D., and Cohen, A. S. (2000) Review: History of the amyloid fibril. *J. Struct. Biol. 130*, 88−98.

(8) Bernstein, S. L., Dupuis, N. F., Lazo, N. D., Wyttenbach, T., Condron, M. M., Bitan, G., Teplow, D. B., Shea, J. E., Ruotolo, B. T., Robinson, C. V., and Bowers, M. T. (2009) Amyloid-β protein oligomerization and the importance of tetramers and dodecamers in the aetiology of Alzheimer's disease. *Nat. Chem. 1*, 326−331.

(9) Quist, A., Doudevski, I., Lin, H., Azimova, R., Ng, D., Frangione, B., Kagan, B., Ghiso, J., and Lal, R. (2005) Amyloid ion channels: A common structural link for protein-misfolding disease. *Proc. Natl. Acad. Sci. U.S.A. 102*, 10427−10432.

(10) Glabe, C. G. (2008) Structural classification of toxic amyloid oligomers. *J. Biol. Chem. 283*, 29639−29643.

(11) DeMuro, A., Smith, M., and Parker, I. (2011) Single-channel Ca^{2+} imaging implicates Aβ1−42 amyloid pores in Alzheimer's disease pathology. *J. Cell Biol. 195*, 515−524.

(12) Lin, H. A. I., Bhatia, R., and Lal, R. (2001) Amyloid β protein forms ion channels: Implications for Alzheimer's disease pathophysiology. *FASEB J. 15*, 2433−2444.
(13) Lashuel, H. A., Hartley, D., Petre, B. M., Walz, T., and Lansbury, P. T. Jr. (2002) Neurodegenerative disease: Amyloid pores from pathogenic mutations. *Nature 418*, 291.
(14) Shirwany, N. A., Payette, D., Xie, J., and Guo, Q. (2007) The amyloid β ion channel hypothesis of Alzheimer's disease. *Neuropsychiatr. Dis. Treat. 3*, 597−612.
(15) Iversen, L. L., Mortishiresmith, R. J., Pollack, S. J., and Shearman, M. S. (1995) The toxicity in-vitro of β-amyloid protein. *Biochem. J. 311*, 1−16.
(16) de Groot, N. S., Aviles, F. X., Vendrell, J., and Ventura, S. (2006) Mutagenesis of the central hydrophobic cluster in Aβ42 Alzheimer's pepticle: Side-chain properties correlate with aggregation propensities. *FEBS J. 273*, 658−668.
(17) Wood, S. J., Wetzel, R., Martin, J. D., and Hurle, M. R. (1995) Prolines and amyloidogenicity in fragments of the Alzheimer's peptide β/A4. *Biochemistry 34*, 724−730.
(18) Williams, A. D., Portelius, E., Kheterpal, I., Guo, J. T., Cook, K. D., Xu, Y., and Wetzel, R. (2004) Mapping Aβ amyloid fibril secondary structure using scanning proline mutagenesis. *J. Mol. Biol. 335*, 833−842.
(19) Walsh, D. M., Lomakin, A., Benedek, G. B., Condron, M. M., and Teplow, D. B. (1997) Amyloid β-protein fibrillogenesis: Detection of a protofibrillar intermediate. *J. Biol. Chem. 272*, 22364−22372.
(20) Bernstein, S. L., Wyttenbach, T., Baumketner, A., Shea, J. E., Bitan, G., Teplow, D. B., and Bowers, M. T. (2005) Amyloid β-protein: Monomer structure and early aggregation states of Aβ42 and its Pro(19) alloform. *J. Am. Chem. Soc. 127*, 2075−2084.
(21) Durell, S. R., Guy, H. R., Arispe, N., Rojas, E., and Pollard, H. B. (1994) Theoretical models of the ion channel structure of amyloid β-protein. *Biophys. J. 67*, 2137−2145.
(22) Arispe, N. (2004) Architecture of the Alzheimer's AβP ion channel pore. *J. Membr. Biol. 197*, 33−48.
(23) Jang, H., Zheng, J., Lal, R., and Nussinov, R. (2008) New structures help the modeling of toxic amyloid β ion channels. *Trends Biochem. Sci. 33*, 91−100.
(24) Shivaprasad, S., and Wetzel, R. (2006) Scanning cysteine mutagenesis analysis of Aβ-(1−40) amyloid fibrils. *J. Biol. Chem. 281*, 993−1000.
(25) Jang, H., Arce, F. T., Ramachandran, S., Capone, R., Azimova, R., Kagan, B. L., Nussinov, R., and Lal, R. (2010) Truncated β-amyloid peptide channels provide an alternative mechanism for Alzheimer's disease and Down syndrome. *Proc. Natl. Acad. Sci. U.S.A. 107*, 6538−6543.
(26) Jang, H., Arce, F. T., Ramachandran, S., Capone, R., Lal, R., and Nussinov, R. (2010) β-Barrel topology of Alzheimer's β-amyloid ion channels. *J. Mol. Biol. 404*, 917−934.
(27) Jang, H., Zheng, J., and Nussinov, R. (2007) Models of β-amyloid ion channels in the membrane suggest that channel formation in the bilayer is a dynamic process. *Biophys. J. 93*, 1938−1949.
(28) Capone, R., Jang, H., Kotler, S. A., Kagan, B. L., Nussinov, R., and Lal, R. (2012) Probing Structural Features of Alzheimer's Amyloid-β Pores in Bilayers Using Site-Specific Amino Acid Substitutions. *Biochemistry 51*, 776−785.
(29) Lührs, T., Ritter, C., Adrian, M., Riek-Loher, D., Bohrmann, B., Doeli, H., Schubert, D., and Riek, R. (2005) 3D structure of Alzheimer's amyloid-β(1−42) fibrils. *Proc. Natl. Acad. Sci. U.S.A. 102*, 17342−17347.
(30) Petkova, A. T., Yau, W. M., and Tycko, R. (2006) Experimental constraints on quaternary structure in Alzheimer's β-amyloid fibrils. *Biochemistry 45*, 498−512.
(31) Zirah, S., Kozin, S. A., Mazur, A. K., Blond, A., Cheminant, M., Segalas-Milazzo, I., Debey, P., and Rebuffat, S. (2006) Structural changes of region 1−16 of the Alzheimer disease amyloid β-peptide upon zinc binding and in vitro aging. *J. Biol. Chem. 281*, 2151−2161.
(32) Capone, R., Jang, H., Kotler, S. A., Connelly, L., Arce, F. T., Ramachandran, S., Kagan, B. L., Nussinov, R., and Lal, R. (2012) All-D-enantiomer of β-amyloid peptide forms ion channels in lipid bilayers. *J. Chem. Theory Comput. 8*, 1143−1152.
(33) Connelly, L., Jang, H., Arce, F. T., Capone, R., Kotler, S. A., Ramachandran, S., Kagan, B. L., Nussinov, R., and Lal, R. (2012) Atomic force microscopy and MD simulations reveal pore-like structures of all-D-enantiomer of Alzheimer's β-amyloid peptide: Relevance to the ion channel mechanism of AD pathology. *J. Phys. Chem. B 116*, 1728−1735.
(34) Brooks, B. R., Bruccoleri, R. E., Olafson, B. D., States, D. J., Swaminathan, S., and Karplus, M. (1983) Charmm: A program for macromolecular energy, minimization, and dynamics calculations. *J. Comput. Chem. 4*, 187−217.
(35) Phillips, J. C., Braun, R., Wang, W., Gumbart, J., Tajkhorshid, E., Villa, E., Chipot, C., Skeel, R. D., Kale, L., and Schulten, K. (2005) Scalable molecular dynamics with NAMD. *J. Comput. Chem. 26*, 1781−1802.
(36) Jang, H., Arce, F. T., Capone, R., Ramachandran, S., Lal, R., and Nussinov, R. (2009) Misfolded amyloid ion channels present mobile β-sheet subunits in contrast to conventional ion channels. *Biophys. J. 97*, 3029−3037.
(37) Jang, H., Arce, F. T., Ramachandran, S., Capone, R., Lal, R., and Nussinov, R. (2010) Structural convergence among diverse, toxic β-sheet ion channels. *J. Phys. Chem. B 114*, 9445−9451.
(38) Smart, O. S., Goodfellow, J. M., and Wallace, B. A. (1993) The pore dimensions of gramicidin A. *Biophys. J. 65*, 2455−2460.
(39) Selkoe, D. J. (2003) Folding proteins in fatal ways. *Nature 426*, 900−904.
(40) Dobson, C. M. (2003) Protein folding and misfolding. *Nature 426*, 884−890.
(41) Roher, A., Wolfe, D., Palutke, M., and KuKuruga, D. (1986) Purification, ultrastructure, and chemical analysis of Alzheimer disease amyloid plaque core protein. *Proc. Natl. Acad. Sci. U.S.A. 83*, 2662−2666.
(42) Cannon, M. J., Williams, A. D., Wetzel, R., and Myszka, D. G. (2004) *Kinetic analysis of β-amyloid fibril elongation*, Vol. *328*, Elsevier, Kidlington, U.K.
(43) Bieschke, J., Siegel, S. J., Fu, Y., and Kelly, J. W. (2008) Alzheimer's Aβ peptides containing an isostructural backbone mutation afford distinct aggregate morphologies but analogous cytotoxicity. Evidence for a common low-abundance toxic structure(s)? *Biochemistry 47*, 50−59.